

Original citation:

Patronis, Alexander and Lockerby, Duncan A.. (2014) Multiscale simulation of non-isothermal microchannel gas flows. Journal of Computational Physics, Volume 270 . pp. 532-543. ISSN 0021-9991

Permanent WRAP url:

<http://wrap.warwick.ac.uk/60260>

Copyright and reuse:

The Warwick Research Archive Portal (WRAP) makes this work of researchers of the University of Warwick available open access under the following conditions.

This article is made available under the Creative Commons Attribution 3.0 (CC BY 3.0) license and may be reused according to the conditions of the license. For more details see: <http://creativecommons.org/licenses/by/3.0/>

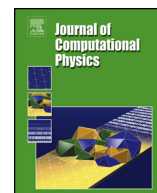
A note on versions:

The version presented in WRAP is the published version, or, version of record, and may be cited as it appears here.

For more information, please contact the WRAP Team at: publications@warwick.ac.uk



<http://wrap.warwick.ac.uk>



Multiscale simulation of non-isothermal microchannel gas flows

Alexander Patronis, Duncan A. Lockerby*

School of Engineering, University of Warwick, UK

ARTICLE INFO

Article history:

Received 20 November 2013

Received in revised form 1 April 2014

Accepted 4 April 2014

Available online 12 April 2014

Keywords:

Multiscale simulation

Rarefied gas dynamics

Thermal transpiration

Thermal creep

Knudsen compressor

Knudsen pump

ABSTRACT

This paper describes the development and application of an efficient hybrid continuum-molecular approach for simulating non-isothermal, low-speed, internal rarefied gas flows, and its application to flows in Knudsen compressors. The method is an extension of the hybrid continuum-molecular approach presented by Patronis et al. (2013) [4], which is based on the framework originally proposed by Borg et al. (2013) [3] for the simulation of micro/nano flows of high aspect ratio. The extensions are: 1) the ability to simulate non-isothermal flows; 2) the ability to simulate low-speed flows by implementing a molecular description of the gas provided by the low-variance deviational simulation Monte Carlo (LVDSMC) method; and 3) the application to three-dimensional geometries. For the purposes of validation, the multiscale method is applied to rarefied gas flow through a periodic converging-diverging channel (driven by an external acceleration). For this flow problem it is computationally feasible to obtain a solution by the direct simulation Monte Carlo (DSMC) method for comparison: very close agreement is observed. The efficiency of the multiscale method, allows the investigation of alternative Knudsen-compressor channel configurations to be undertaken. We characterise the effectiveness of the single-stage Knudsen-compressor channel by the pressure drop that can be achieved between two connected reservoirs, for a given temperature difference. Our multiscale simulations indicate that the efficiency is surprisingly robust to modifications in streamwise variations of both temperature and cross-sectional geometry.

© 2014 The Authors. Published by Elsevier Inc. This is an open access article under the CC BY license (<http://creativecommons.org/licenses/by/3.0/>).

1. Introduction

Designers of microfluidic devices are in need of computational tools that can be used to analyse problems that involve rarefied gas flows in complex micro geometries. Numerical simulation of the gas flow through such geometries is, however, extremely challenging. Conventional continuum fluid dynamics (CFD) becomes invalid or inaccurate as the characteristic scale of the geometry (e.g. the channel height, h) approaches the molecular mean free path, λ [1,2]. When $\lambda/h \gtrsim 0.1$, the error in solutions obtained from CFD may be significant, and we must consider the fluid for what it is: a collection of interacting particles. However, the computational expense of simulating the flow of a rarefied gas in high-aspect-ratio micro geometries (i.e. ones that are long, relative to their cross section) using a particle method, such as the direct simulation Monte Carlo (DSMC) method [2], can be prohibitively high [3,4]. The computational intensity of the particle method

* Corresponding author.

E-mail address: d.lockerby@warwick.ac.uk (D.A. Lockerby).

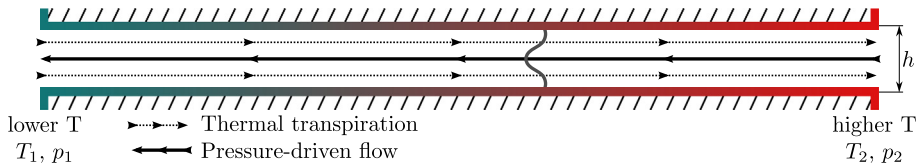


Fig. 1. Thermal transpiration and opposing pressure-driven flow.

is greater still when simulating low-speed microfluidic devices where there are only small deviations from equilibrium, characterised by extremely low Mach numbers and weak temperature gradients.

To simulate the flow of a rarefied gas in micro geometries of high aspect ratio, processes need to be resolved simultaneously over both the smallest and largest characteristic length scales of the geometry: the problem is multiscale in nature. To tackle this, the internal-flow multiscale method (IMM) [3] has been developed. The IMM facilitates the coupling of conventional continuum theory and a suitable particle method, via mass and momentum flux conservation. This coupling allows us to take advantage of the simplicity and efficiency of continuum theory, and the accuracy of the particle method. The IMM is iterative, involving a bidirectional and indirect exchange of information between the continuum domain and a number of spatially-distributed particle subdomains, until convergence is obtained.

Recently, the IMM has been extended to treat compressible internal rarefied gas flows [4], but limited to isothermal problems and relatively high-speed flows. The DSMC method was used to provide the molecular description of the gas transport, and thus low-speed near-equilibrium flows could not be simulated efficiently. This is because, at low speeds, the number of samples required to obtain an acceptable signal-to-noise ratio is intractable.

In this paper, we present two extensions to the IMM that enable: a) non-isothermal and b) near-equilibrium flows to be modelled. We apply this extended IMM to study the phenomenon of thermal transpiration, and its application to Knudsen compressors (also known as Knudsen pumps) [5]: solid-state thermal molecular pumps which operate by exploiting thermal transpiration.

Thermal transpiration (thermal creep) is a rarefied gas effect, whereby a slip flow is generated at a surface in response to a streamwise variation in temperature. Importantly, and counter-intuitively, flow is driven from lower temperature to higher temperature regions. Fig. 1 illustrates the steady-state flow field in a channel with height comparable to the molecular mean free path, which connects two reservoirs; one with temperature T_1 and pressure p_1 , and the other with temperature T_2 and pressure p_2 . In this steady state, the net mass flow rate through the channel is zero. The transient processes that result in this steady-state condition are not captured by the IMM, but are briefly described here for clarity. Initially, with zero tangential wall-temperature gradient, $p_1 = p_2$. As a tangential wall-temperature gradient is applied, fluid is transported by thermal transpiration into the reservoir with high temperature. This raises the pressure in the high-temperature reservoir, creating a pressure gradient opposing the thermal transpiration. This pressure gradient continues to develop until it is sufficient to fully balance the flow due to thermal transpiration, resulting in zero mass flow rate (see Fig. 1). To achieve a large pressure drop ($p_2 - p_1$), the flow resistance must be high, and so typically the aspect ratio of the channel must be high.

2. Multiscale and numerical methodology

The internal-flow multiscale method (IMM), which was developed for high-aspect-ratio geometries, uses particle-based ‘micro subdomains’, covering the full cross section of the channel or tube. These subdomains are distributed in the streamwise direction with a spacing sufficient to resolve any streamwise variation in the simulation geometry and flow variables within it. This subdomain placement is illustrated in Fig. 2(b), for a generic internal-flow geometry, Fig. 2(a). The geometry of each subdomain represents the cross-sectional geometry of the macro domain at that point locally.

Application of the IMM requires that a degree of length-scale separation exists between hydrodynamic variation along streamlines (i.e. in the s -direction, see Fig. 2(a)) and microscopic processes transverse to the flow direction (in x - and y -directions). For this scale separation to exist, the section geometry (and the wall boundary conditions) must vary slowly in the streamwise direction. A dimensionless number indicating the degree of such scale separation can be expressed:

$$S = \min \left\{ \left| \frac{dL_y}{ds} \right|^{-1}, \left| \frac{dL_z}{ds} \right|^{-1}, \left| \frac{L_y}{\phi} \frac{d\phi}{ds} \right|^{-1}, \left| \frac{L_z}{\phi} \frac{d\phi}{ds} \right|^{-1}, \left| \frac{R_y}{L_y} \right|, \left| \frac{R_z}{L_z} \right| \right\}, \quad (1)$$

where L_y and L_z are length scales in the transverse directions that characterise the cross-section geometry, ϕ is a flow variable (e.g., density, temperature or pressure), and R_y and R_z are the radii of curvature of the centre streamline. Provided $S \gg 1$, it can safely be assumed that, in small streamwise sections of the tube/channel, streamwise flow variations are effectively negligible and the walls are approximately parallel to the centre streamline (and consequently all other local streamlines). This is referred to by Borg et al. [3] as a *local parallel-flow assumption*, and it allows for the simulation domain to be represented by streamwise-periodic subdomains with exactly parallel walls, as depicted in Fig. 2(b). Depending on the type of molecular solver utilised, these subdomains can be three-dimensional (with a small but finite dimension in the s -direction) as illustrated in Fig. 2(b), or two-dimensional, as is the case in this paper, where the subdomains are cross-sectional slices with no dimension in the s -direction.

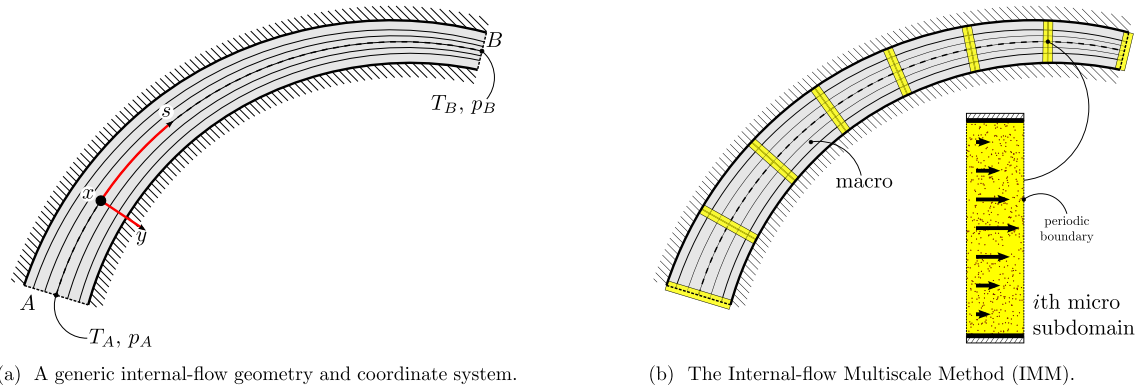


Fig. 2. Schematics of (a) a generic internal-flow geometry and (b) the internal-flow multiscale method (IMM) [3,4]. A molecular description of the fluid (DSMC, LVDSMC, MD, etc.) is used for the highlighted regions, as illustrated for the i th micro subdomain.

Given low Reynolds number, isothermal, and locally-parallel flow, the flow conditions at any streamwise position in the channel can be fully defined by: the gas density, the tangential wall velocities, and the streamwise pressure gradient (which is generated in streamwise-periodic subdomains by an effective body force). In this paper, we extend the IMM to include the non-isothermal properties of temperature and streamwise temperature gradient. This development provides a means to study the phenomenon of thermal transpiration and its application to Knudsen compressors.

In these problems, the gas temperature and streamwise temperature gradient at any point are fixed by the boundary conditions at the wall; for low Mach number flows in high-aspect-ratio channels there will be a negligible variation in temperature through the channel cross section. Thus, the role of the IMM in the context of thermal transpiration flows is to determine the impact of an applied streamwise temperature variation on mass flow rate and pressure/density variation through the simulation domain.

2.1. Macro–micro coupling

For the thermal transpiration flows considered here, all that is needed to define the flow state in a particular subdomain is the wall temperature and streamwise temperature gradient (both known from boundary conditions), and the density (ρ) and streamwise pressure gradient (Φ) at that position in the full domain. The latter two variables are calculated by coupling the subdomain micro models and a macroscopic description of the flow field; the macro model is simply mass conservation through the full domain. The macro–micro coupling is simply stated as:

$$\langle \dot{m}_i \rangle = \dot{M} \quad \text{for } i = 1, 2, \dots, \Pi, \quad (2)$$

where $\langle \dot{m}_i \rangle$ is the mass flow rate measured from the i th of Π subdomains, and \dot{M} is the macroscopic mass flow rate through the entire geometry.

The IMM follows an iterative procedure, predicting values of Φ and ρ in each subdomain which generate micro mass-flow responses that will ultimately satisfy Eq. (2) once convergence is reached. On convergence, the macro mass flow rate and the streamwise distribution of density and pressure gradient constitute the output of the method.

The iterative solution of Eq. (2) requires some prediction of the general response of the mass flow rate in each subdomain to changes in Φ and ρ . To this end, it is assumed that the mass flow rate is separately proportional to the net momentum flux and the streamwise temperature gradient:

$$\dot{m}_i = k_i(\rho_i a_{\text{ext}} - \Phi_i) + j_i \left. \frac{dT}{ds} \right|_i, \quad (3)$$

where i denotes a value at the i th subdomain, T is the gas temperature and a_{ext} is any externally-applied acceleration. The constant of proportionality k_i is estimated prior to the first iteration; as will be seen, the constant j_i determining the mass flow rate due to thermal transpiration does not require estimation. Note, the prediction in Eq. (3) is approximate at the micro scale for rarefied gas flows. However, the accuracy of the prediction only determines convergence characteristics of the method and does not affect the final solution (provided one can be found).

Eq. (3) is used to estimate the change in mass flow rate between successive iterations:

$$\dot{m}_i^{l+1} - \langle \dot{m}_i^l \rangle = k_i(\rho_i^{l+1} a_{\text{ext}} - \rho_i^l a_{\text{ext}} - \Phi_i^{l+1} + \Phi_i^l), \quad (4)$$

where l is the iteration index and angular brackets denote a value measured from the subdomains. Note, the thermal transpiration term has been eliminated by assuming it is unaffected by changes in density and pressure gradient. The simulations of [6] demonstrate that this assumption is questionable under certain conditions. However, as noted above, the

inaccuracy in this assumption only affects the rate of convergence of the iterative scheme, and not the final solution of the IMM.

To make the mass flow rates in each subdomain tend to a single macroscopic value we substitute \dot{m}_i^{l+1} for \dot{M} :

$$\dot{M} + k_i(\Phi_i^{l+1} - \rho_i^{l+1} a_{\text{ext}}) = \langle \dot{m}_i^l \rangle + k_i(\Phi_i^l - \rho_i^l a_{\text{ext}}). \quad (5)$$

As Φ and ρ converge ($\rho^{l+1} \rightarrow \rho^l$ and $\Phi^{l+1} \rightarrow \Phi^l$), Eq. (5) ensures macro mass conservation is satisfied, i.e., $\langle \dot{m}_i^l \rangle \rightarrow \dot{M}$. We focus on ideal gases, allowing the expression of the pressure gradient in terms of density and temperature:

$$\Phi_i^{l+1} = RT_i \left. \frac{d\rho}{ds} \right|_i^{l+1} + R \left. \frac{dT}{ds} \right|_i \rho_i^{l+1} \quad (6)$$

where R is the specific gas constant.

At each iteration, Eqs. (5) and (6) are solved simultaneously, producing sequentially improving predictions for \dot{M} , Φ_i , and ρ_i ; the latter two variables are then re-applied to the micro subdomain solvers. As is clear from Eq. (6), a discrete representation of the derivative of density is required (the derivative of temperature is defined directly by the wall boundary conditions, as discussed previously). As in [4], we adopt a spectral collocation method for high accuracy; an example of this numerical scheme for non-periodic problems is presented in Appendix A.

2.2. Boundary conditions

The solution of Eqs. (5) and (6) requires two boundary conditions, in addition to those of temperature and tangential velocity at the walls of the full domain. The obvious choice, and those adopted in Borg et al. [3] and Patronis et al. [4], are boundary conditions on inlet pressure and outlet pressure ($p_1 = p_A$, $p_\Pi = p_B$; see Fig. 2(a)). However, for the Knudsen compressor problem, see Fig. 1, the equilibrium pressure drop (the steady-state condition when the pressure-driven flow balances the thermal transpiration flow) is not known *a priori*. In this instance we set a condition on mass flow rate ($\dot{M} = 0$) and upstream pressure ($p_1 = p_A$), while the pressure downstream becomes an output of the simulation. This ability to invert the problem demonstrates a new advantage of the IMM over a full-domain molecular simulation.

2.3. Micro model: low-variance deviational particle Monte Carlo (LVDSMC)

The direct simulation Monte Carlo method suffers from overwhelming statistical scatter in hydrodynamic variables when simulating near-equilibrium, rarefied gas flows, such as those encountered in individual Knudsen compressors. Therefore, unlike in Patronis et al. [4] a variance reduced deviational particle method for simulating the Boltzmann transport equation for the variable hard sphere (VHS) collision operator has been adopted (source code freely available at [7]). This method has been successfully applied to a range of applications, see Refs. [8,9] for full details. Referred to as low-variance deviational simulation Monte Carlo (LVDSMC), this technique overcomes the limitations of the DSMC method when used to simulate small deviations from equilibrium. The key to achieving variance reduction by LVDSMC (and deviational particle methods in general), is the decomposition of the velocity distribution into an equilibrium state, which can be represented analytically, and a deviational distribution, which is represented in terms of simulated particles. For the same number of particles (simulators), that would otherwise have been used to simulate the entire velocity distribution, the deviational distribution can be simulated with dramatically lower variance.

An additional attractive feature of the LVDSMC method is that it enables the simulation of small streamwise gradients in pressure and temperature without the added expense and complexity of simulating a non-periodic streamwise-extending domain [10]. The equivalent effects of these streamwise gradients are introduced conveniently by an effective body force [10]; a technique first proposed by Cercignani [11]. Importantly, this allows the application of streamwise gradients in pressure (Φ_i) and temperature ($\frac{dT}{ds}|_i$) independently of each other, in each subdomain.

It is important to note that other micro models could be employed that would be equally accurate for the purposes of the IMM, while being computationally cheaper than LVDSMC. For example, numerical solutions to linearised kinetic equations can be performed extremely efficiently (see, e.g. [12]). However, here we have chosen the LVDSMC method for the convenience that a particle method affords, and to allow easy extension to arbitrary cross-sectional geometries at a later date.

2.4. Coupling algorithm

Each iteration of the IMM generates a sequence of improving approximate values at collocation points (at each micro subdomain) for mass density and pressure gradient. Once converged, the mass flow rates in each subdomain are equal and macroscopic mass is conserved. The iterative method ceases to execute once a convergence criterion (e.g. on standard deviation of the mass flow rates measured from the micro subdomains) is satisfied. The iterative method follows the procedure outlined below:

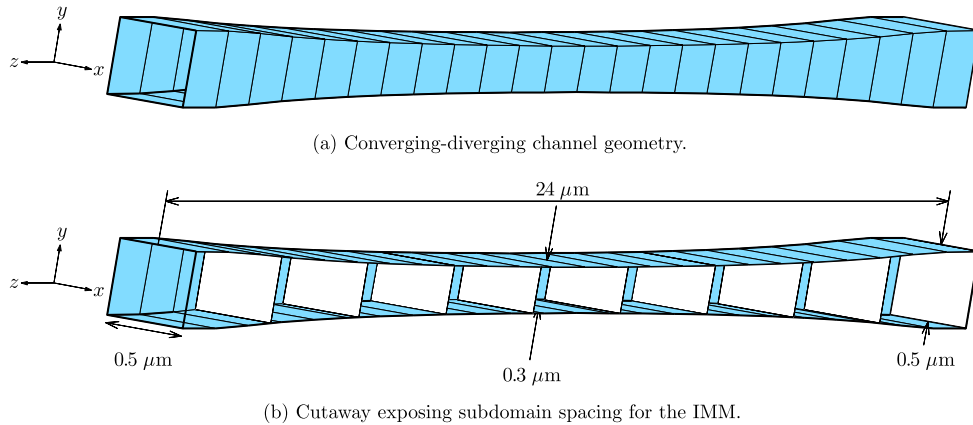


Fig. 3. A streamwise periodic converging-diverging channel.

1. Initialise all micro LVDSMC (subdomain) simulations with the density and pressure gradient values for the current iteration: ρ_i^l , Φ_i^l , and the temperature T_i and temperature gradient $\frac{dT}{ds}|_i$ dictated by the wall boundary conditions for that subdomain location.
2. Simulate all Π micro LVDSMC subdomains in two stages: a transient period and an averaging period. The transient period allows for the flow simulated in each subdomain to reach steady state. A satisfactory signal-to-noise ratio for the mass flow rate measurement, $\langle \dot{m}_i^l \rangle$, is then obtained during the averaging period.
3. Solve the set of linear Eqs. (5) and (6) (in discretised form: (A.6), (A.7) and (A.8)) satisfying the boundary conditions to obtain density and pressure gradient values for the next iteration: ρ_i^{l+1} , Φ_i^{l+1} .
4. Repeat from (1) until Eq. (2) is satisfied (i.e. macroscopic mass conservation is attained).

Prior to initiation of the iterative algorithm, a set of Π simulations (one for each subdomain) must be performed in order to generate values of k_i . This is achieved by applying a zero temperature gradient and an arbitrary pressure gradient Φ_i in each subdomain. The mass flow rate measured from each subdomain is then used to obtain values of k_i directly from Eq. (3).

3. LVDSMC-IMM validation

In this section we test the integrity of the newly-proposed IMM of this paper (i.e. the IMM with the LVDSMC method providing micro resolution) by comparing with full-domain simulation results obtained from the far-more computationally intensive DSMC method. Although the DSMC method is a numerical method, it is appropriate as a reference for validation because: a) the DSMC method has been thoroughly validated against experimental data and theoretical results, as has the particular solver used (dsmcFoam, [13–15]); and b) we are primarily concerned with the ability of the IMM to reproduce the same result but at a fraction of the computational cost. The dsmcFoam solver is available as part of the open source CFD software package, OpenFOAM, which is freely available at [16].

The validation case consists of a three-dimensional converging-diverging channel, with periodicity in the streamwise direction; the configuration is shown in Fig. 3. The flow is driven by a uniform and constant acceleration a_{ext} . The length of the channel is $L_s = 24 \mu\text{m}$, the height at the throat is $\min(h) = 0.3 \mu\text{m}$ and the height at the inlet/outlet is $\max(h) = 0.5 \mu\text{m}$, the width of the cross section (in the x -direction) is a constant $w = 0.5 \mu\text{m}$. The aspect ratio of the channel is: $L_s/w = 48$. For this isothermal test case, the temperature of all surfaces representing walls is kept constant at $T_{\text{wall}} = 273 \text{ K}$, and the average density in the domain is initialised at $\rho = 0.573 \text{ kg m}^{-3}$. For both the full-domain simulation computed by the DSMC method and all micro LVDSMC (subdomain) simulations, a VHS model of argon is used, and the size of all computational cells is chosen to be considerably smaller than the local mean free path.

The full-domain dsmcFoam simulation is performed using a time-step that is a small fraction of the mean free time (the mean time between collisions): $\Delta t = 2 \times 10^{-11} \text{ s}$. Each cell contains an initial 50 representative particles to produce a total number of 6.8×10^6 simulators. These simulators represent $\sim 3.81 \times 10^7$ real particles in the system. Time averaging was activated at $t = 1 \times 10^{-6} \text{ s}$ and continued until $t = 3 \times 10^{-5} \text{ s}$, producing 1.45 million samples. The applied external acceleration is $a_{\text{ext}} = 10^{10} \text{ m s}^{-2}$; a value chosen to produce a manageable signal-to-noise ratio. Despite this strong acceleration, the maximum Reynolds number $\text{Re} = 0.22$ (based on local centreline velocity and local channel height, h), and the maximum Mach number $\text{Ma} = 0.045$. The Knudsen number (at the centreline) ranges from $\text{Kn} = 0.32$ – 0.63 ($\text{Kn} = \lambda/h$), as shown in Fig. 4. An IMM simulation of the geometry is performed with $\Pi = 9$ equally-spaced subdomains: the positions of the subdomains are shown in Fig. 3(b). Note, each subdomain is in fact a transverse plane, having no dimension in the s -direction.

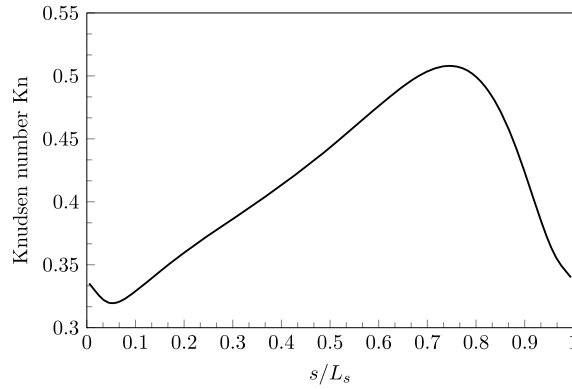


Fig. 4. Variation of the Knudsen number (based on y -dimension) in the streamwise direction, s .

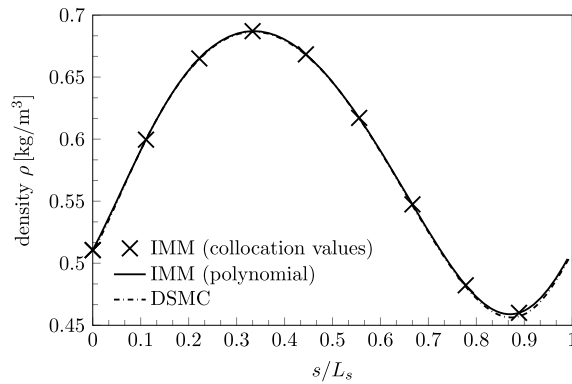


Fig. 5. Comparison of streamwise variation of mass density computed by the dsmcFoam solver (---) applied to the full domain, and the (LVDSMC-)IMM (—X—). The collocation points, X, are also shown.

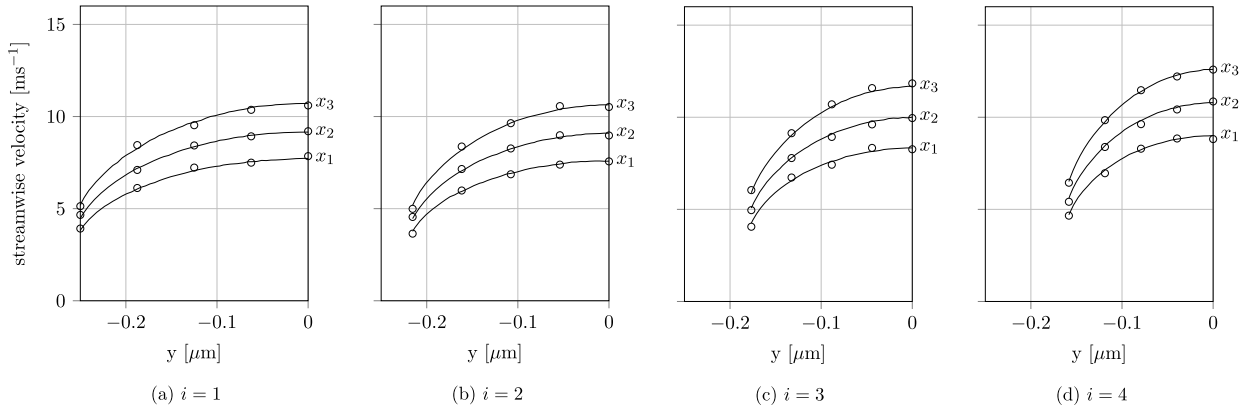


Fig. 6. Profiles of fluid velocity at various streamwise locations (a)–(d) and at three transverse slices located at, $x = x_1, x_2, x_3$. Circular markers represent velocity profiles computed by the dsmcFoam solver. Solid lines represent velocity profiles obtained by the compressible (LVDSMC-)IMM method. $x_1 = -0.204 \mu\text{m}$; $x_2 = -0.153 \mu\text{m}$; $x_3 = 0 \mu\text{m}$; (a) $i = 1$ ($s/L_s = 0$); (b) $i = 2$ ($s/L_s = 0.111$); (c) $i = 3$ ($s/L_s = 0.222$); (d) $i = 4$ ($s/L_s = 0.333$). Wall locations are: (a) $x = \pm 0.25 \mu\text{m}$, $y = \pm 0.25 \mu\text{m}$; (b) $x = \pm 0.25 \mu\text{m}$, $y = \pm 0.216 \mu\text{m}$; (c) $x = \pm 0.25 \mu\text{m}$, $y = \pm 0.177 \mu\text{m}$; (d) $x = \pm 0.25 \mu\text{m}$, $y = \pm 0.158 \mu\text{m}$.

A comparison of the results obtained from the LVDSMC-IMM and the full-domain dsmcFoam simulation is presented in Figs. 5 and 6. Fig. 5 shows the streamwise variation of mass density (at the centreline) through the domain, and Fig. 6 compares velocity profiles at four different streamwise locations, each at three different transverse slices (x locations). Agreement is excellent between the results of the IMM and those of the full-domain dsmcFoam simulation. What is perhaps counter-intuitive from the results presented in Fig. 5 is that the density is not constant despite the low Mach number (this fluid-compressibility effect was seen in Patronis et al. [4], and its occurrence in micro flows is discussed in [17]). Furthermore, the position of maximum density does not occur at the throat of the channel, but instead slightly upstream.

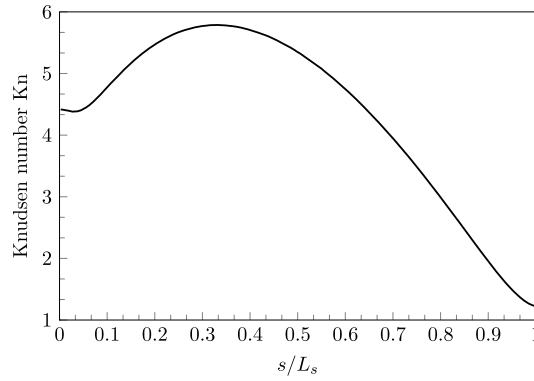


Fig. 7. Variation of the Knudsen number (based on y -dimension) in the streamwise direction, s .

Both the full-domain dsmcFoam simulation and the IMM predict this. Note, the difference in the velocity-profile resolution seen in Fig. 6 exists because a larger cell size is used to simulate the full domain using dsmcFoam; i.e. resolution was sacrificed for the purposes of averaging. The mass flow rate measured by dsmcFoam is $\dot{m} = 1.01 \pm 0.11 \times 10^{-12} \text{ kg s}^{-1}$; the mass flow rate calculated from the converged (LVDSMC-)IMM is $\dot{m} = 1.0085 \pm 0.0015 \times 10^{-12} \text{ kg s}^{-1}$.

The LVDSMC-IMM boasts a considerable reduction in computational intensity relative to the full-domain dsmcFoam simulation. To assess the computational performance of the LVDSMC-IMM and full-domain dsmcFoam, we compare the wall-clock time required by the LVDSMC-IMM to iterate until the convergence criterion is satisfied, and the wall-clock time required for dsmcFoam to compute a steady and low-noise pressure and velocity field. We take the convergence criterion of the IMM to be:

$$|\text{stdev}\{\dot{m}_i\}/\overline{\dot{m}_i^1}| < \zeta_{\text{tol}}, \quad (7)$$

where $\overline{\dot{m}_i^1}$ is the mean of the mass flow rates measured during the first iteration, and ζ_{tol} is a predetermined tolerance. For the simulations in this paper we choose: $\zeta_{\text{tol}} = 0.002$.

For consistency in comparison, all simulations for both methods are performed using Intel Xeon X5650 2.66 GHz cores. The LVDSMC-IMM utilises a single Intel Xeon X5650 2.66 GHz core per subdomain, and therefore requires 9 cores per iteration for the current case. Since an iteration cannot be completed until all subdomain simulations of that iteration have ended, the subdomain simulations of any iteration are executed in parallel to maximise efficiency. The wall-clock time required by the LVDSMC-IMM to iterate until the convergence criterion is satisfied is $\sim 4.90h$. To obtain a satisfactory solution using the dsmcFoam solver, 64 cores are required for $\sim 49.8h$. Based on wall-clock time, the full-domain dsmcFoam simulation is approximately 10 times more expensive than the LVDSMC-IMM. In terms of ‘core-hours’, the LVDSMC-IMM is over 70 times cheaper than the full-domain simulation: a major reduction of computational intensity. This saving is due to: a) the IMM allows the full three-dimensional domain to be represented as a small number of planar surfaces; and b) the LVDSMC method is more efficient than the DSMC method, even at moderate flow speeds ($\sim 10 \text{ m s}^{-1}$).

4. Application to Knudsen-compressor channels

In this section we apply the LVDSMC-IMM to the channel flow depicted in Fig. 1, where thermal-transpiration flow is balanced by an opposing pressure-gradient driven flow. This equilibrated steady-state response is representative of that encountered in Knudsen-compressor channels, and is therefore of technological interest. The IMM promises to make the simulation of more general geometries and temperature variations accessible to design exploration. For all cases in this section, the gas considered is VHS argon.

4.1. Straight channel with linear temperature profile

In the first case, we consider a thermal transpiration flow driven by a linear streamwise wall-temperature gradient. The length of the straight channel is $L_s = 24 \mu\text{m}$, with a square cross section of height $h = 0.5 \mu\text{m}$. The streamwise temperature distribution is given by $T(s) = -3.75 \times 10^7(s) + 1000 \text{ K}$.¹ The Knudsen number of the flow (at the centreline) ranges from $\text{Kn} = 2.05$ – 5.79 , as shown in Fig. 7; the pressure at the inlet, p_A , is $\sim 8.07 \times 10^3 \text{ Pa}$.

¹ The temperature change over the length of the $24 \mu\text{m}$ channel is of the order of 900 K. Such a high gradient of temperature may be technologically impractical, and has been chosen here primarily for the purpose of creating a computationally challenging example.

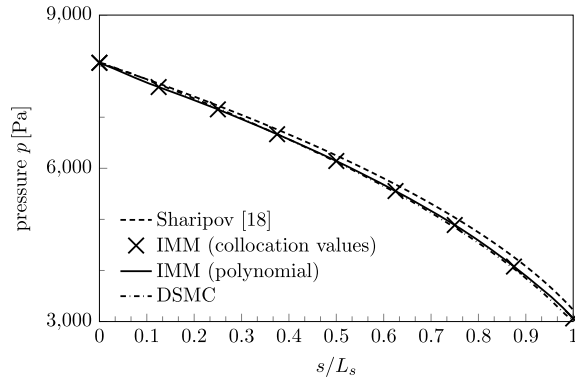


Fig. 8. Comparison of streamwise variation of pressure computed by the dsmcFoam solver (— · —) applied to the full domain, the (LVDSMC-)IMM (×), and the method outlined by Sharipov [18] (---). The collocation points, ×, are also shown.

The IMM simulation of the channel is performed with $\Pi = 9$ evenly-distributed subdomains. For comparison, a full-domain simulation using the DSMC method is performed ($\Delta t = 1 \times 10^{-11}$ s). Each cell contains an initial 80 representative particles to produce a total number of 2×10^5 simulators. Due to the prohibitive computational expense, we do not attempt to resolve the velocity profiles using the DSMC method. Similarly, we do not use the DSMC method to calculate the downstream pressure producing zero net flow rate, as this would need to be found by trial-and-error.² Instead, the pressure boundary conditions of the full-domain dsmcFoam simulation are set based on the solution from the IMM, and only the predictions of streamwise variation in pressure are compared.

We also present the streamwise variation of pressure as calculated by the model proposed by Sharipov [18]:

$$\frac{dp}{ds} = \frac{Q_T(\delta)}{Q_p(\delta)} \frac{p(s)}{T(s)} \frac{dT}{ds} \quad (8)$$

where δ is the rarefaction parameter (inverse of the Knudsen number), and values for the coefficients Q_p and Q_T are obtained from the S-model kinetic equation [19]. Here, Eq. (8) is solved using a Runge–Kutta method, with values of Q_p and Q_T at any given δ found by cubic interpolation between values published in Sharipov [18].

Fig. 8 shows the streamwise variation of pressure (at the centreline) through the domain, as computed by the IMM, the dsmcFoam solver, and the approximate solution of Sharipov [18]. These methods indicate a non-linear pressure variation being generated by the application of the linear temperature gradient. This reflects the effect of the varying Knudsen number on the thermal transpiration flow. As expected, the streamwise variation of pressure computed by applying the method of Sharipov [18] deviates slightly from that obtained by applying the other methods, due to the approximation inherent in the S-model kinetic equation. Fig. 9 shows the velocity profiles obtained from the IMM at three different streamwise locations. The inverted flow profile, resulting from the opposing effects of the pressure gradient and the thermal transpiration, is clearly observed. These results provide confidence that the LVDSMC-IMM can be applied to investigate more general non-isothermal Knudsen compressor flows.

4.2. Straight channel with non-linear temperature profile

In this section, we apply the IMM to determine whether a greater pressure drop can be achieved by altering the temperature distribution, whilst maintaining the same total temperature drop. For the purposes of this investigation, this is our gauge of efficiency. All simulation conditions applied here are identical to those used to simulate the previous case, except that a non-linear temperature profile is prescribed. The temperature distribution is given by $T(s) = 1.20 \times 10^{12}(s)^2 - 66.3 \times 10^6(s) + 1000$ K for case 1, and $T(s) = -1.20 \times 10^{12}(s)^2 - 8.70 \times 10^6(s) + 1000$ K for case 2; see Fig. 10. Note, the total temperature drop is the same in both cases. The IMM is applied to calculate the pressure distribution that satisfies $\dot{M} = 0$, i.e. a zero net mass flow rate in the domain. Fig. 11 shows the pressure distributions for case 1 and case 2 computed by the IMM (—) and the model outlined by Sharipov (---). It is clear, and perhaps unexpected, that the total pressure drop is relatively unaffected by the temperature distribution. In case 1, a 62% change in pressure is observed; in case 2 this is 61.6% change in pressure. In some sense this result demonstrates the robustness of the Knudsen compressor: it is not necessary to precisely apply a surface temperature gradient to achieve a desired pressure drop. The model of Sharipov also captures this.

² As discussed in Section 2.2, the IMM has the advantage of allowing zero mass flow rate in the domain to be set in place of a boundary condition on pressure.

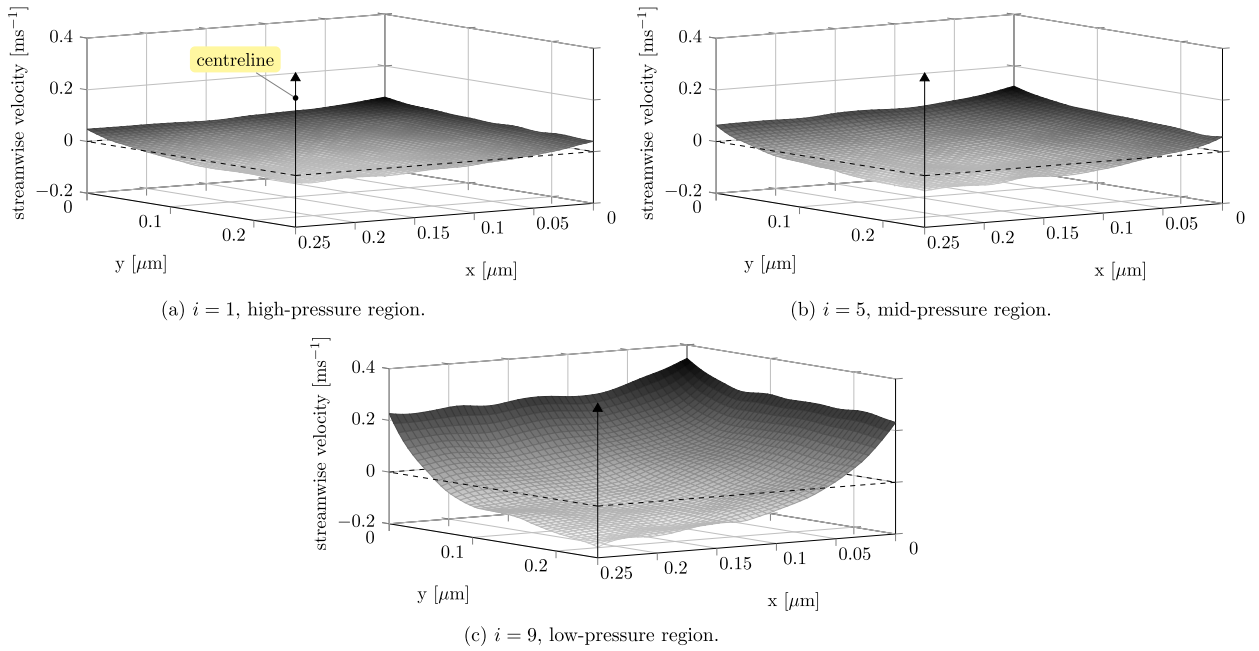


Fig. 9. Profiles of fluid velocity (in the direction of thermal transpiration) in the transverse plane. (a) $i = 1$ ($s/L_s = 0$); (b) $i = 5$ ($s/L_s = 0.5$); (c) $i = 9$ ($s/L_s = 1$). Wall location: $x = 0, 0.5 \mu\text{m}$, $y = 0, 0.5 \mu\text{m}$. Due to symmetries in the x - and y -directions, only a quarter of the subdomain is simulated.

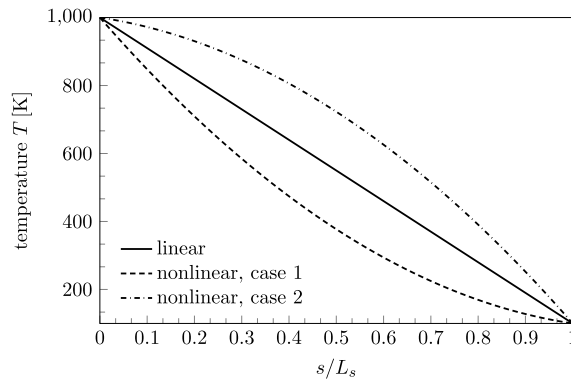


Fig. 10. Linear temperature profiles applied in Section 4.1 and non-linear temperature profiles applied in Section 4.2.

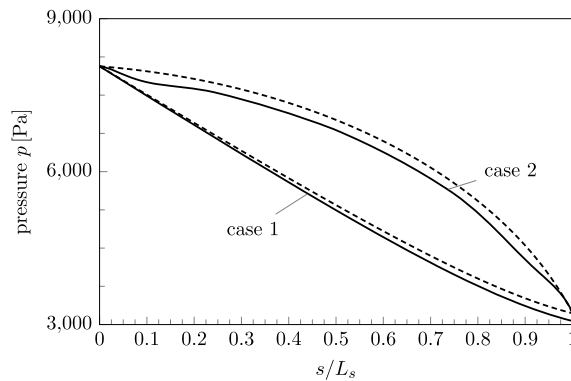


Fig. 11. Comparison of streamwise variation of pressure for cases 1 and 2, computed by the (LVDSMC)-IMM (—), and the method outlined by Sharipov [18] (----).

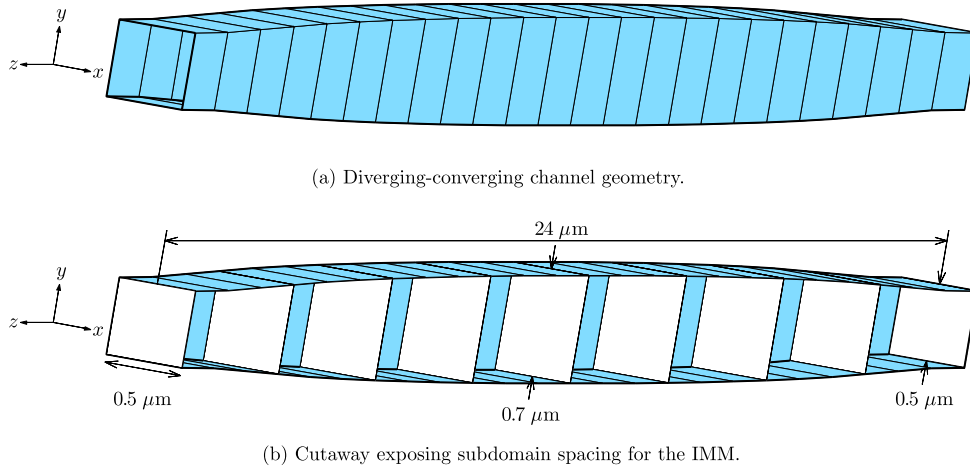


Fig. 12. Variation of the Knudsen number (based on y -dimension) in the streamwise direction, s , for: converging-diverging channel (—), and diverging-converging channel (----).

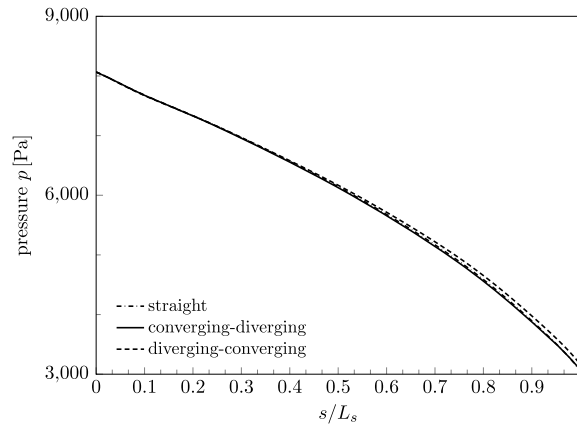


Fig. 13. Streamwise variation of pressure for: straight channel (----), converging-diverging channel (—), and diverging-converging channel (----).

4.3. Non-uniform channel geometry with linear temperature gradient

We now use the IMM to investigate whether modifications to the cross-sectional geometry (in the streamwise direction) can influence the total pressure drop attainable. This exploration cannot be performed easily using the Sharipov model of Eq. (8). Here we apply the linear temperature profile defined in Section 4.1. All simulation conditions applied here are identical to those used to simulate the previous case described in Section 4.1. Note, the total temperature drop is the same in both cases.

We consider two non-uniform channels: case 1) a three-dimensional converging-diverging channel (see Fig. 3(a)) and case 2) a three-dimensional diverging-converging channel (see Fig. 12), both with non-periodic boundary conditions. The IMM is applied to calculate the pressure distribution that satisfies $\dot{M} = 0$, i.e. a zero net mass flow rate in the domain. Fig. 13 shows the pressure distributions for these cases. As in the cases of the previous section, the total pressure drop appears to be relatively unaffected by the very significant modification to the cross-sectional geometry. In case 1, a 61.9% change in pressure is observed; in case 2 this is 60.7% change in pressure. This result further points to a rather surprising robustness of the Knudsen-compressor channel design to the pressure drop achieved.

5. Conclusions

This paper describes the development of a number of major extensions to the compressible internal-flow multiscale method (IMM) [4]. These extensions have been made, in part, to allow the study of Knudsen-compressor channel flows. The extensions are: 1) ability to simulate *non-isothermal* internal rarefied gas flows; 2) ability to simulate low-speed flows by adopting a molecular description of the gas provided by the low-variance deviational simulation Monte Carlo (LVDSMC) method; and 3) application to three-dimensional simulation domains. We have applied the method to dilute gas flows (using

the VHS-LVDSMC method to provide micro resolution) for periodic and non-periodic internal-flow configurations, and to the study of thermal transpiration. For validation purposes, the solution from the IMM has been compared to that obtained from a full-domain simulation using the dsmcFoam solver. The IMM provides flow predictions that are in excellent agreement with those from the full-domain simulations. More importantly, the IMM is significantly more efficient, resulting in major computational savings in all cases. The IMM has been used to investigate how streamwise variations in temperature and cross-sectional geometry can affect Knudsen-compressor performance. It was found that the overall pressure difference that is obtained is fairly insensitive to such modifications. This potentially demonstrates a robustness of the Knudsen-compressor performance to some aspects of channel design.

Future work in extending the applicability of the LVDSMC-IMM will be to accommodate flow regions of low aspect ratio, i.e. where scale separation doesn't exist. In such regions a full micro solution of the low-aspect-ratio region needs to be coupled to the scale-separated treatment of the high-aspect-ratio flow. Details of how this can be done for nanofluidic networks comprising both high-aspect-ratio and low-aspect-ratio internal flow components are given in [20], where a Molecular Dynamics micro model has been used.

Acknowledgements

This work is financially supported by the EPSRC Grants EP/I011927/1 and EP/K038664/1. The authors would like to thank Craig White for providing an updated version of the dsmcFoam source code, and Nicolas Hadjiconstantinou for providing the LVDSMC source code, available at [7].

Appendix A. Spectral collocation scheme

To investigate the thermal transpiration phenomenon, a non-periodic configuration with pressure boundary conditions must be used. However, as will be explained, it is not necessary to prescribe boundary values of pressure at both inlet and outlet. Readers are referred to [4] for a full description of the collocation scheme that is applied to solve periodic problems.

The density variation in a non-periodic domain is represented by the following polynomial:

$$\rho(s) = \sum_{j=0}^{\Pi} \hat{\rho}_j s^j, \quad (\text{A.1})$$

where $\hat{\rho}_0, \dots, \hat{\rho}_{\Pi}$ are the coefficients of the polynomial. From Eq. (6), a polynomial description of Φ is:

$$\Phi(s) = RT(s) \sum_{j=1}^{\Pi} j \hat{\rho}_j s^{j-1} + R \frac{dT(s)}{ds} \sum_{j=0}^{\Pi} \hat{\rho}_j s^j. \quad (\text{A.2})$$

Eq. (A.2) includes the contribution of the temperature gradient to the streamwise pressure-gradient. Eqs. (A.1) and (A.2) are evaluated at the subdomain locations (collocation points):

$$s_i = L_s(i-1)/(\Pi-1) \quad \text{for } i = 1, 2, \dots, \Pi \quad (\text{A.3})$$

which encompass the full length of the geometry, to give variables in physical space at the new iteration:

$$\rho_i^{l+1} = \sum_{j=0}^{\Pi} \hat{\rho}_j s_i^j, \quad (\text{A.4})$$

$$\Phi_i^{l+1} = RT_i \sum_{j=1}^{\Pi} j \hat{\rho}_j s_i^{j-1} + R \left. \frac{dT}{ds} \right|_i \sum_{j=0}^{\Pi} \hat{\rho}_j s_i^j, \quad (\text{A.5})$$

where Eq. (A.4) requires $\Pi + 1$ coefficients for the degree Π polynomial. Eqs. (A.4) and (A.5) are substituted into Eq. (5) to obtain:

$$\dot{M} + k_i \left[\left(RT_i \sum_{j=1}^{\Pi} j \hat{\rho}_j s_i^{j-1} + R \left. \frac{dT}{ds} \right|_i \sum_{j=0}^{\Pi} \hat{\rho}_j s_i^j \right) - \left(\sum_{j=0}^{\Pi} \hat{\rho}_j s_i^j \right) a_{\text{ext}} \right] = \langle \dot{m}_i^l \rangle + k_i (\Phi_i^l - \rho_i^l a_{\text{ext}}), \quad (\text{A.6})$$

where the iteration indices of the coefficients are omitted for clarity. Eq. (A.6) represents Π equations containing $\Pi + 2$ unknowns. The two remaining equations required for its solution are obtained from the boundary conditions on pressure at the inlet and outlet:

$$p_1 = RT_1 \hat{\rho}_0, \quad (\text{A.7})$$

and

$$p_{\Pi} = RT_{\Pi} \sum_{j=0}^{\Pi} \hat{\rho}_j L_s^j, \quad (\text{A.8})$$

where L_s is the total streamwise length of the geometry. The set of linear equations (A.6), (A.7) and (A.8) can be solved at each iteration using LU decomposition, or similar. After each iteration, the variables at collocation points (in physical space) can be obtained from Eqs. (A.4) and (A.5).

An alternative method of solution is to introduce a mass flow rate condition in place of one of the pressure boundary conditions (A.7) or (A.8). For example:

$$\dot{M} = 0. \quad (\text{A.9})$$

References

- [1] J.M. Reese, M.A. Gallis, D.A. Lockerby, New directions in fluid dynamics: non-equilibrium aerodynamic and microsystem flows, *Philos. Trans. R. Soc., Math. Phys. Eng. Sci.* 361 (2003) 2967–2988.
- [2] G.A. Bird, *Molecular Gas Dynamics and the Direct Simulation of Gas Flows*, Oxford University Press, Oxford, UK, 1994.
- [3] M.K. Borg, D.A. Lockerby, J.M. Reese, A multiscale method for micro/nano flows of high aspect ratio, *J. Comput. Phys.* 233 (2013) 400–413.
- [4] A. Patronis, D.A. Lockerby, M.K. Borg, J.M. Reese, Hybrid continuum-molecular modelling of multiscale internal gas flows, *J. Comput. Phys.* 255 (2013) 558–571.
- [5] S.E. Vargo, E.P. Muntz, G.R. Shiflett, W.C. Tang, Knudsen compressor as a micro- and macroscale vacuum pump without moving parts or fluids, *J. Vac. Sci. Technol. A* 17 (1999) 2308–2313.
- [6] H. Akhlaghi, E. Roohi, Mass flow rate prediction of pressure-temperature-driven gas flows through micro/nanoscale channels, *Contin. Mech. Thermodyn.* 26 (2014) 67–78.
- [7] Massachusetts Institute of Technology, Hadjiconstantinou, <http://web.mit.edu/ngh-group/research3-variance.html>, 2011.
- [8] T.M.M. Homolle, N.G. Hadjiconstantinou, A low-variance deviational simulation Monte Carlo for the Boltzmann equation, *J. Comput. Phys.* 226 (2007) 2341–2358.
- [9] G.A. Radtke, N.G. Hadjiconstantinou, W. Wagner, Low-noise Monte Carlo simulation of the variable hard sphere gas, *Phys. Fluids* 23 (2011) 30606.
- [10] G.A. Radtke, Efficient simulation of molecular gas transport for micro- and nanoscale applications, Ph.D., Massachusetts Institute of Technology, 2011.
- [11] C. Cercignani, A. Daneri, Flow of a rarefied gas between two parallel plates, *J. Appl. Phys.* 34 (1963) 3509–3513.
- [12] D. Valougeorgis, S. Naris, Acceleration schemes of the discrete velocity method: gaseous flows in rectangular microchannels, *SIAM J. Sci. Comput.* 25 (2003) 534–552.
- [13] C. White, M.K. Borg, T.J. Scanlon, J.M. Reese, A DSMC investigation of gas flows in micro-channels with bends, *Comput. Fluids* 71 (2013) 261–271.
- [14] E. Arlemark, G. Markelov, S. Nedeia, Rebuilding of Rothe's nozzle measurements with OpenFOAM software, *J. Phys. Conf. Ser.* 362 (2012) 12040.
- [15] T.J. Scanlon, E. Roohi, C. White, M. Darbandi, J.M. Reese, An open source, parallel DSMC code for rarefied gas flows in arbitrary geometries, *Comput. Fluids* 39 (2010) 2078–2089.
- [16] OpenFOAM Foundation, OpenFOAM – the open source computational fluid dynamics (CFD) toolbox, 2014; <http://www.openfoam.org>.
- [17] M. Gad-el Hak (Ed.), *MEMS: Introduction and Fundamentals*, CRC Press, 2005.
- [18] F. Sharipov, Non-isothermal gas flow through rectangular microchannels, *J. Micromech. Microeng.* 9 (1999) 394.
- [19] E.M. Shakhov, Generalization of the Krook kinetic relaxation equation, *Fluid Dyn.* 3 (1968) 95–96.
- [20] M.K. Borg, D.A. Lockerby, J.M. Reese, A hybrid molecular-continuum simulation method for incompressible flows in micro/nanofluidic networks, *Micronfluid. Nanofluid.* 15 (2013) 541–557.